Research Square

Preprints are preliminary reports that have not undergone peer review.
They should not be considered conclusive, used to inform clinical practice,
or referenced by the media as validated information.

# Arctic-wide freshwater outburst from the Baltic Ice Lake contributed to the onset of Preboreal cooling

**Dhanushka Devendra**

devendra@iopan.pl

Institute of Oceanology Polish Academy of Sciences https://orcid.org/0000-0003-1005-1621

**Magdalena Łącka**

Institute of Oceanology Polish Academy of Sciences

**Natalia Szymańska**

Institute of Oceanology Polish Academy of Sciences

**Małgorzata Szymczak-Żyła**

Institute of Oceanology Polish Academy of Sciences

**Magdalena Krajewska**

Institute of Oceanology Polish Academy of Sciences

**Maciej Telesiński**

Institute of Oceanology Polish Academy of Sciences https://orcid.org/0000-0002-5765-2849

**Prasadi De Silva**

Institute of Oceanology Polish Academy of Sciences

**Tine Rasmussen**

UiT the Arctic University of Norway

**Katarzyna Melaniuk**

UiT The Arctic University of Norway

**Marek Zajączkowski**

Institute of Oceanology Polish Academy of Sciences

**Article**

**Keywords:** Preboreal Oscillation, freshwater, Atlantic Water, sea ice, biomarkers, lake outburst, European Arctic

**Posted Date:** July 1st, 2026

**DOI:** https://doi.org/10.21203/rs.3.rs-10164525/v1

**License:** This work is licensed under a Creative Commons Attribution 4.0 International License.
Read Full License

**Additional Declarations:** There is **NO** Competing Interest.

# Arctic-wide freshwater outburst from the Baltic Ice Lake contributed to the onset of Preboreal cooling

Dhanushka Devendra[1]*, Magdalena Łącka[1], Natalia Szymańska[1], Małgorzata Szymczak-Żyła[1], Magdalena Krajewska[1], Maciej M. Telesiński[1], Prasadi De Silva[1], Tine L. Rasmussen[2], Katarzyna Melaniuk[2], Marek Zajączkowski[1]

[1] Department of Paleoceanography, Institute of Oceanology, Polish Academy of Sciences, Sopot 81-712, Poland

[2] Department of Geosciences, UiT The Arctic University of Norway, Tromsø, Norway

* *correspondence to:* Dhanushka Devendra (devendra@iopan.pl)

## Abstract

Freshwater pulses from proglacial lakes are considered key drivers of past ocean circulation and climate variability, but they remain poorly constrained. Here, we investigate their role during the early Holocene by applying a suite of independent proxies to three high-resolution sedimentary records from the southwestern Barents Sea. Freshwater inputs are reconstructed from $\%C_{37:4}$ and benthic foraminiferal $\delta^{18}O$, sea-surface temperature from the $U^{K*}_{37}$ index, and sea-ice conditions from $IP_{25}$ and $PIP_{25}$. Changes in paleoproductivity and phytoplankton community response to freshwater forcing are assessed using phytoplankton-derived sterols. We identified three regionally coherent freshwater events affecting the Nordic Seas, including a major event between ~11.5 and 11 kyr BP. This interval shows pronounced surface-water freshening, cooling, and expanded sea-ice cover that aligns with independent regional chronologies. Its timing and hydrographic signature closely align with the Baltic Ice Lake outburst, suggesting that its discharge was a significant freshwater source driving the Preboreal cooling. Our findings reveal that the influence of this outburst extended farther into the Arctic than previously recognised, highlighting its broader role in early Holocene ocean-climate dynamics.

**Keywords.** Preboreal Oscillation; freshwater; Atlantic Water; sea ice; biomarkers; lake outburst; European Arctic

## 1. Introduction

Freshwater pulses have had a distinct and dramatic impact on the climate and oceanography of the European Arctic [1, 2, 3, 4, 5]. Reconstructing these events and understanding their repercussions is particularly significant in the context of modern climate change, as similar freshwater discharges from melting large ice sheets are increasingly anticipated [2, 6]. Numerous recent modeling studies have attempted to predict the consequences of such freshwater discharges from the Antarctic and Greenland ice sheets [7, 8, 9, 10]. Some predict a substantial weakening or even a shutdown of the Atlantic Meridional Overturning Circulation (AMOC), which could lead to severe global climatic consequences e.g[11].

The Preboreal Oscillation (PBO), a distinct and short-lived cooling event of approximately 250 years, occurred around 11.3 kyr BP, and remains challenging to constrain precisely using $^{14}C$ dating [12]. Well documented in high-resolution terrestrial and marine archives across the North Atlantic region e.g[12, 13, 14, 15, 16], the event is thought to have been triggered by a large freshwater influx into the higher-latitude North Atlantic, which weakened the AMOC and thereby led to regional cooling [15, 17]. Despite its short duration, the PBO represents a critical moment in the transition from the Last Glacial Maximum to the Holocene, highlighting the sensitivity of the North Atlantic climate system to shifts driven by freshwater forcing. Understanding the PBO is essential for reconstructing past climate dynamics, as it provides insights into how large-scale hydrological events can influence both the regional and global climate system. However, the exact source of this freshwater pulse remains poorly constrained and has not been thoroughly discussed in the literature.

Major lakes drainage events from both Lake Agassiz and Baltic Ice Lake (BIL) occurred close to the onset of PBO [14, 15, 17], and these outbursts have long been considered a potential freshwater source capable of triggering the event. Most previous interpretations, however, relied heavily on the choice of limited proxy records and remain inconclusive regarding the dominant source of freshwater. Fisher, Smith [17] proposed that the PBO was initiated by a catastrophic drainage from Lake Agassiz, expansion of sea ice, and the southward advection of low-salinity surface water from the Arctic Ocean into the North Atlantic, rather than by an increased flux of freshwater from the Nordic region. Despite this apparent consensus, the precise origin of the freshwater pulses remains unresolved, with multiple potential drainage sources proposed and no clear agreement across proxy records. To clarify this issue, we present comprehensive proxy records of seawater conditions, with

freshwater inputs reconstructed from $\%C_{37:4}$ and benthic foraminiferal $\delta^{18}O$, sea-surface temperature from the $U^{K*}_{37}$ index, and sea-ice conditions from $IP_{25}$ and $PIP_{25}$. These records are derived from three sediment cores retrieved from the southwestern Barents Sea, alongside previously published records from the Barents Sea and Norwegian continental margin (Fig. 1).

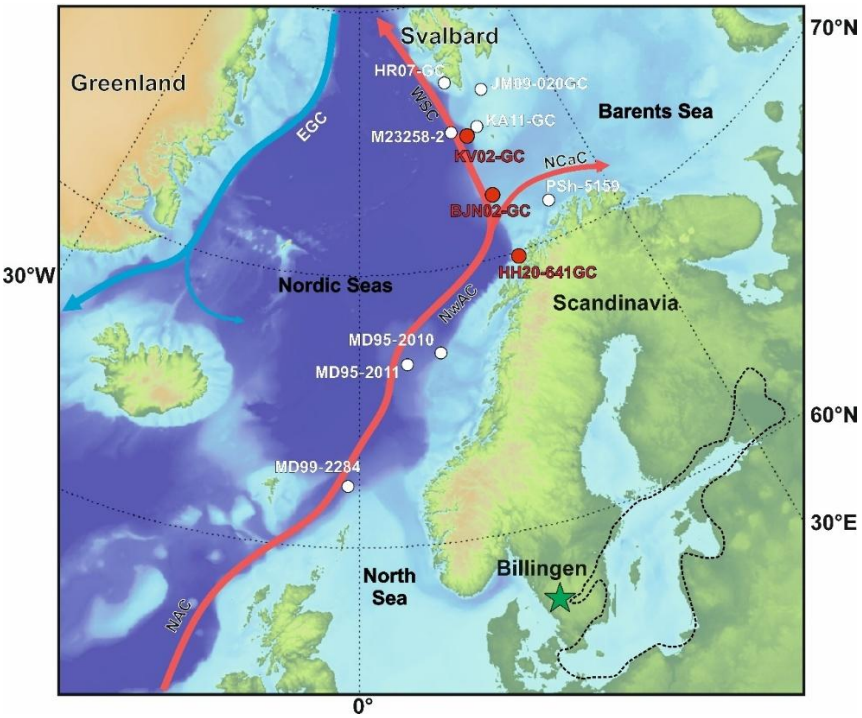



**Figure 1: Present-day surface ocean circulation in the Nordic Seas.** Locations of marine sediment cores from this study (red circles) and reference cores (white circles) mentioned in the text: OCE2022-KV02-GC (this study), OCE2023-BJN02-GC (this study), HH20-641GC (this study), M23258-2 [18, 19], KA11-GC [20], HR07-GC [13], JM09-020-GC [21], PSh-5159 [22], MD95-2010 [23], MD95-2011 [24], and MD99-2284 [25]. The dashed polygon represents the estimated extent of the Baltic Ice Lake, modified from Harrison, Smith [2], at ~11.5 kyr BP. The green star marks Mount Billingen. Red arrows indicate the pathways of warm Atlantic Water, including North Atlantic Current (NAC), Norwegian Atlantic Current (NwAC), North Cape Current (NCaC), and West Spitsbergen Current (WSC). The blue arrow indicates the East Greenland Current (EGC). The map was generated using GeoMapApp version 3.7.5 (http://www.geomapapp.org) [26].

## 2. Results and Discussion

### Early Holocene freshwater discharges to the western Barents Sea

We use the percentage of tetra-unsaturated alkenone ($\%C_{37:4}$) to trace freshwater release at our study sites e.g[27]. $C_{37:4}$ is produced by the seawater coccolithophore species *Emiliania huxleyi* at low

temperatures [28], but can also be produced by other alkenone producers living in low-salinity waters [27, 29]. Recent studies suggest that $\%C_{37:4}$ may serve as an indicator of sea-ice, as alkenones can also be synthesized by coccolithophores living in sea-ice, with $\%C_{37:4}$ values reaching up to ~80% [30]. However, according to our records, $C_{37:4}$ is not the dominant alkenone (averaging <20%), suggesting that open-water algae production influenced by freshwater is the most likely source of alkenones in this area. Moreover, in the Nordic Seas, the proportion of $C_{37:4}$ has been shown to respond mainly to changes in salinity, particularly when it exceeds 5% [31]. Accordingly, we interpret the $\%C_{37:4}$ signal recorded in this study as a proxy for changes in freshwater influence.

$\%C_{37:4}$ values exhibit high variability, particularly between ~13 and ~9 kyr BP, in our nothernmost studied cores (Fig. 2). Elevated $\%C_{37:4}$ values across the Bølling–Allerød (BA) and Younger Dryas (YD) transition suggest a substantial freshwater supply to the western Barents Sea (Fig. 2). Following the transition interval, we identified three distinct and rapid increases in $\%C_{37:4}$ values, likely corresponding to freshtwater pulses (FP). We refer to these pulses as FP1, FP2, and FP3, which occurred approximately 12.4–12 kyr BP, 11.5–11.1 kyr BP, and 10.3–9.7 kyr BP, respectively. Among them, FP2 is particularly significant compared to the other two events and likely coincides with the PBO cooling (Fig. 2).

Although all three events were primarily identified from the KV02-GC core, distinct increases in $\%C_{37:4}$ were also observed in the BJN02-GC core, corresponding to the identified freshtwater events (Fig. 2). Moreover, a notable decrease in benthic $\delta^{18}O$ during these intervals further supports our interpretation of freshening in the western Barents Sea (Fig. 2). Additional evidence for freshwater influence during FP2 is provided by HH20-641GC record. Although the HH20-641GC record only covers the interval between ~13 and ~10.8 kyr BP, it captures a pronounced decrease in benthic $\delta^{18}O$ synchronous with FP2, indicating rapid freshening of bottom waters during this interval. Importantly, the pronounced benthic $\delta^{18}O$ decrease observed at HH20-641GC (272 m water depth), together with similar signals in KV02-GC (374 m) and BJN02-GC (375 m), suggests that freshwater influence penetrated much of the water column, consistent with a substantial freshwater perturbation of the western Barents Sea.

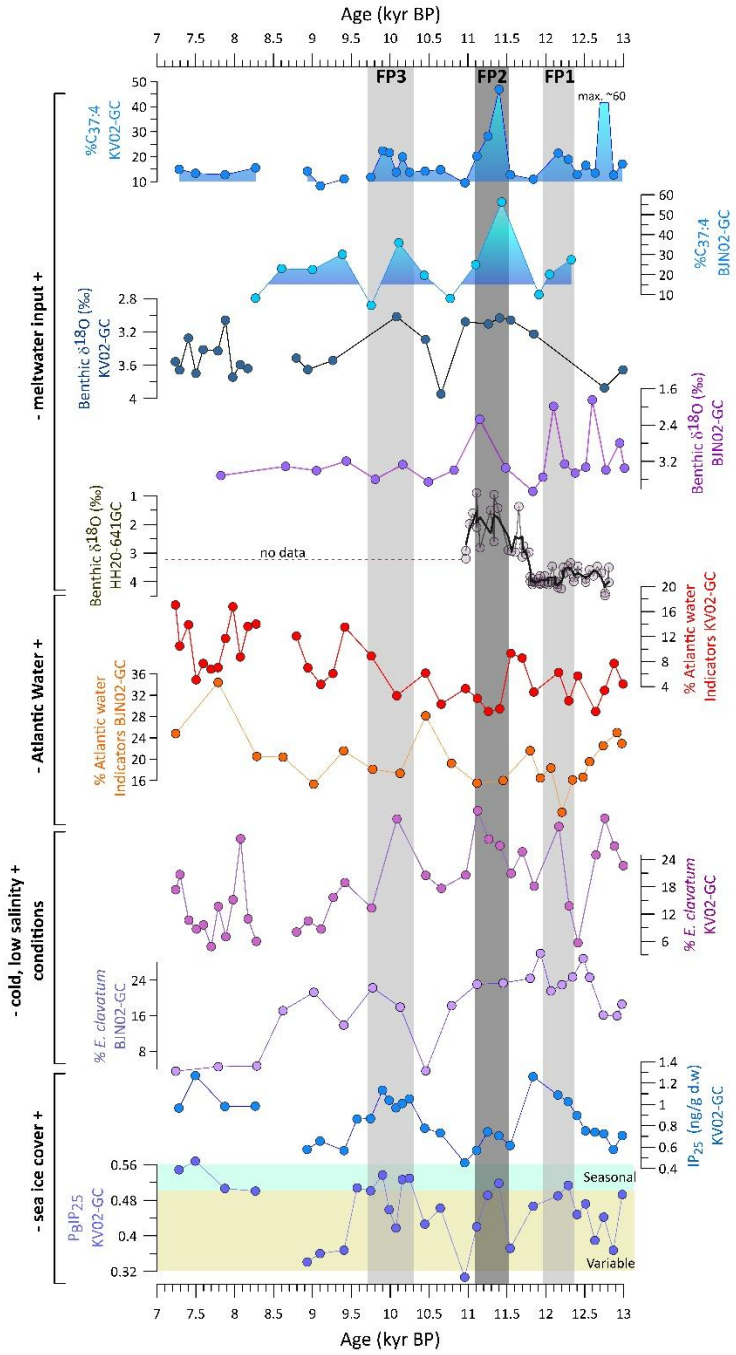



**Figure 2. Multiproxy indicators of freshwater input, water-mass variability, and sea-ice conditions across freshwater events (FP1–FP3)**. Downcore records of the tetra-unsaturated alkenone fraction ($\%C_{37:4}$), benthic $\delta^{18}O$, the relative abundance of the Atlantic Water indicator (*Cassidulina neoteretis*), the relative abundance of *Elphidium clavatum*, and $IP_{25}$ and $PBIP_{25}$ (sea-ice indicators) are plotted against age (kyr BP). Gray vertical bars indicate freshwater events FP1–FP3 identified in this study, with the darker bar marking the Preboreal Oscillation -related event. $IP_{25}$ is present throughout all three phases, while $P_BIP_{25}$ remains within a narrow range, indicating persistent seasonal sea-ice conditions. Variations in benthic $\delta^{18}O$, Atlantic Water indicators, and *E. clavatum* abundance illustrate changes in bottom-water properties and surface-water salinity associated with freshwater input during each

perturbation phase. The data-free interval in KV02-GC corresponds to a reworked sediment layer identified by Devendra, Łącka [32].

The consistent elevation of $\%C_{37:4}$ values and corresponding benthic $\delta^{18}O$ decreases in multiple studied cores suggests that these events were not isolated, but rather part of a broader regional freshwater signal affecting the western Barents Sea and adjacent Nordic Seas. The expression of these freshwater proxies reinforces the interpretation that these events were synchronous, reflecting large-scale hydrographic reorganizations and freshwater routing events in the North European Arctic margin.

## Implications of freshwater pulses on the western Barents Sea environment

Several abrupt changes in environmental conditions were observed during freshwater discharges into the western Barents Sea. The events are marked by abrupt shifts in oceanographic conditions, including increased presence of seasonal sea-ice – as evidenced by elevated $IP_{25}$ and intermediate $P_BIP_{25}$ values– alongside decreased sea surface temperatures and a reduced influx of AW into the western Barents Sea margin (Figs. 2 and 3). The reduced AW contribution is reflected by the lower abundance of AW indicator species *Cassidulina neoteretis* and lower benthic $\delta^{18}O$ values (Fig. 2). While lower benthic $\delta^{18}O$ values point to reduced AW inflow [33], they also suggest a direct influence of low salinity waters reaching the seafloor. Such conditions are consistent with a freshwater-driven deepening of the halocline [34], potentially forcing warm AW masses further westward, away from our study area. Elevated abundances of *Elphidium clavatum* during these freshwater events (Fig. 2) further support increased freshwater influence and reduced bottom water salinity e.g[35].

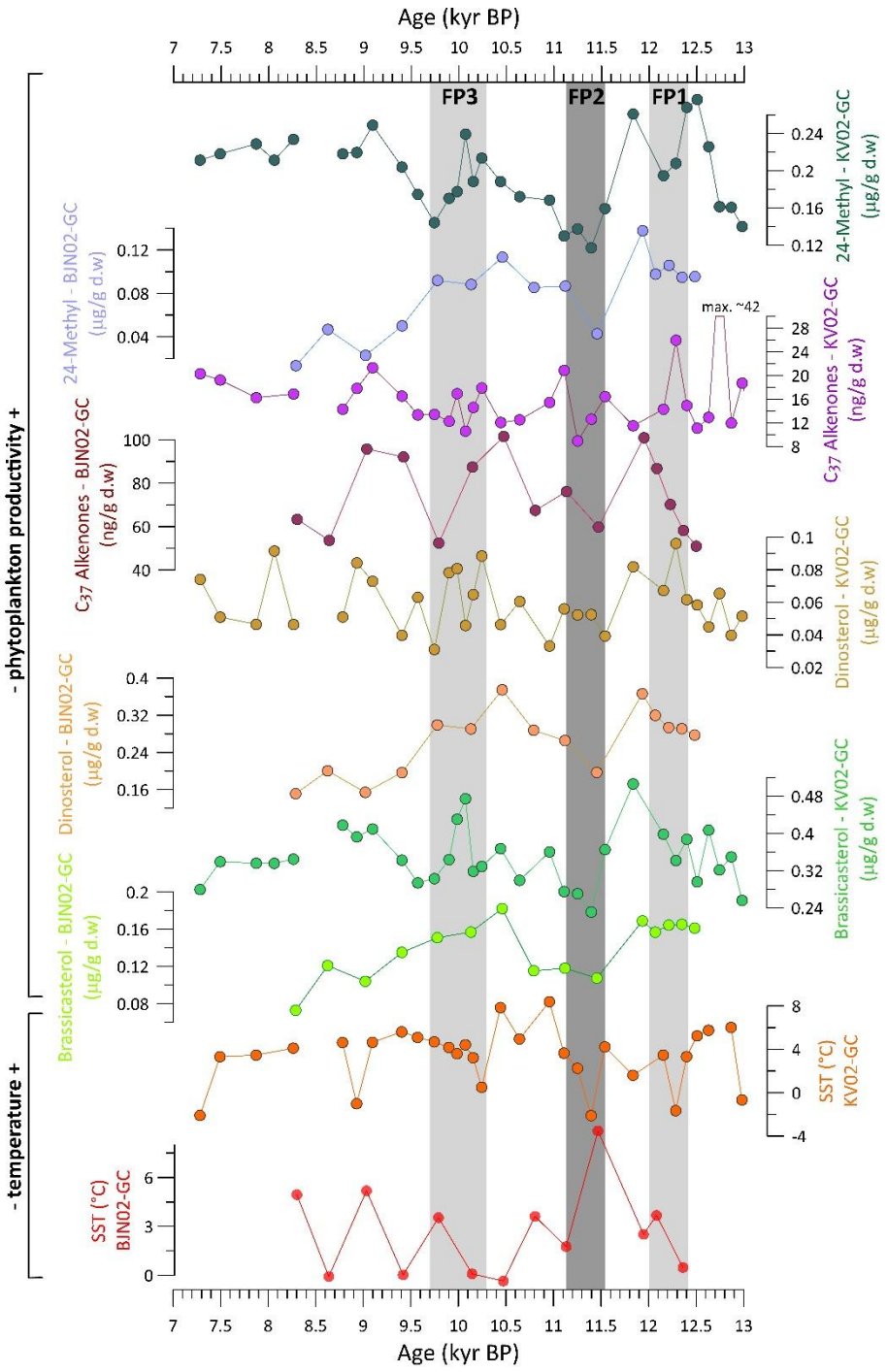



**Figure 3. Productivity and sea-surface conditions across freshwater perturbation events (FP1–FP3).** Downcore variations in marine productivity proxies from cores KV02-GC and BJN02-GC plotted against age (kyr BP). Shown are concentrations of 24-methylenecholesterol, $C_{37}$ alkenones ($\Sigma C_{37}$), dinosterol, and brassicasterol, together with reconstructed sea-surface temperature (SST). Blue vertical bars indicate freshwater events FP1–FP3 identified in this study, with the darker bar marking the Preboreal Oscillation-related event. FP1 and FP3 coincide with enhanced productivity proxies, whereas FP2, occurring during the Preboreal Oscillation, is marked by exceptionally

high freshwater influence and a pronounced suppression of marine primary productivity across all biomarker groups, despite comparable seasonal sea-ice conditions ($PBIP_{25}$ ~0.5; see Fig. 2). The data-free interval in KV02-GC corresponds to a reworked sediment layer identified by Devendra, Łącka [32].

All three freshwater perturbation events in our records (FP1, FP2, and FP3) occurred under seasonal sea-ice conditions, as indicated by intermediate $P_BIP_{25}$ values (~0.5; Fig. 2) [36], and are associated with pronounced surface freshening. Despite this common context, FP1 during the late YD and FP3 in the Preboreal interval exhibit elevated concentrations of total alkenones ($\Sigma C_{37}$) and phytoplankton-derived sterols, including brassicasterol, 24-methylenelcholesterol, and dinosterol (Fig. 3). These signals indicate enhanced productivity of haptophytes, diatoms, and dinoflagellates, respectively [37, 38, 39]. Comparatively elevated $IP_{25}$ concentrations during FP1 and FP3 are consistent with seasonal sea ice conditions, while the co-occurrence of freshwater input and sustained surface primary productivity suggests that vertical mixing and nutrient availability were not substantially suppressed. Such conditions are compatible with productive marginal ice zone or sea-ice edge environments, where freshwater input can coexist with enhanced primary production e.g[40].

In contrast, FP2, occurring during the PBO, exhibits a fundamentally different environmental response. This event is characterized by exceptionally high $\%C_{37:4}$ values together with markedly reduced $\Sigma C_{37}$ and sterol biomarker concentrations (Figs. 2 and 3), indicating substantial suppression of marine primary productivity across multiple phytoplankton groups. Although $IP_{25}$ is present, its relatively low concentration compared to FP1 and FP3 suggests that extensive or persistent sea-ice cover was not the primary driver of the productivity decline. Instead, the combined biomarker evidence indicates that enhanced freshwater-induced stratification and reduced nutrient supply to the surface waters are the primary mechanisms driving ecosystem suppression during FP2. The contrasting behavior of FP2 relative to the other two events demonstrates that freshwater discharge can produce fundamentally different ecosystem outcomes even under comparable seasonal ice conditions, highlighting the sensitivity of high-latitude marine ecosystems to background climatic states.

The distinctive environmental response associated with FP2, characterized by extreme surface freshening, weakened AW influence, and a pronounced suppression of marine primary productivity, suggests that this event reflects a perturbation extending beyond a purely local response. Its clear divergence from FP1 and FP3 under comparable seasonal sea-ice conditions points to a broader-scale reorganization of oceanographic conditions affecting the western Barents

Sea. In the following section, we therefore examine the regional expression of the PBO by comparing FP2 in our cores with other marine and terrestrial records, to assess the spatial coherence, timing, and magnitude of this event across the wider North Atlantic-European Arctic region.

**Regional expression and correlation of the Preboreal Oscillation**

To assess the climatic relevance of our identified freshwater events, we compared the timing of these signals with regional climate archives from the Norwegian and Barents Sea continental margin (60°–75°N; Fig. 1). Though all three identified events are closely synchronized with regional hydrological anomalies, here we focus primarily on FP2 since several studies have documented hydrological changes that broadly overlap with this event e.g[13, 15, 19, 22, 24, 25, 41, 42].

The FP2 event (11.5 – 11.1 kyr BP) aligns with the well-documented PBO, a ~ 250-year cooling event centered around 11.3 kyr BP (11.4–11.27 kyr BP). In the Nordic Seas, the PBO is characterized by lowered sea surface temperatures, expanded sea-ice cover, increased freshwater input, and reduced Atlantic Water inflow. Our data show a strong temporal correspondence with these hydrographic shifts, as we observed substantial freshening and cooling, in agreement with regional records (Figs. 4 and 5). Specifically, our alkenone-based SST estimates show a ~3 °C cooling in the western Barents Sea, with a similar trend reflected in other regional SST records (Fig. 5). Notably, the southmost record (core MD99-2284 from the southwestern Norwegian Sea) shows a ~5 °C cooling based on foraminifera-derived SSTs (Fig. 5), together with increased abundances of *Neogloboquadrina pachyderma* (Fig. S1). The planktic $\delta^{18}O$ values from the same site suggest substantial freshening of the surface water column, a signal also evident in other $\delta^{18}O$ records across the region (Fig. 4). This freshening likely strengthened water column stratification, which in turn could have affected bottom water hydrography, including temperatures e.g[34, 43], and is reflected in lighter benthic $\delta^{18}O$ records from deep-sea cores (cores MD99-2284 and MD95-2010; Fig. S1).

In addition, decreases in $\delta^{18}O$, coupled with elevated $\%C_{37:4}$ in cores PSh-5159, MD95-2010, M23258-2, HR07-GC, and JM09-020GC, suggest that the freshening during FP2 was not a local anomaly but part of a broader regional hydrological reorganization (Fig. 4). These concurrent signals strongly indicate that FP2 corresponds to a prominent, regionally expressed freshtwater event that aligns with the hydrographic perturbations associated with the PBO, and may itself have acted as a potential freshwater source contributing to the initiation of the PBO.

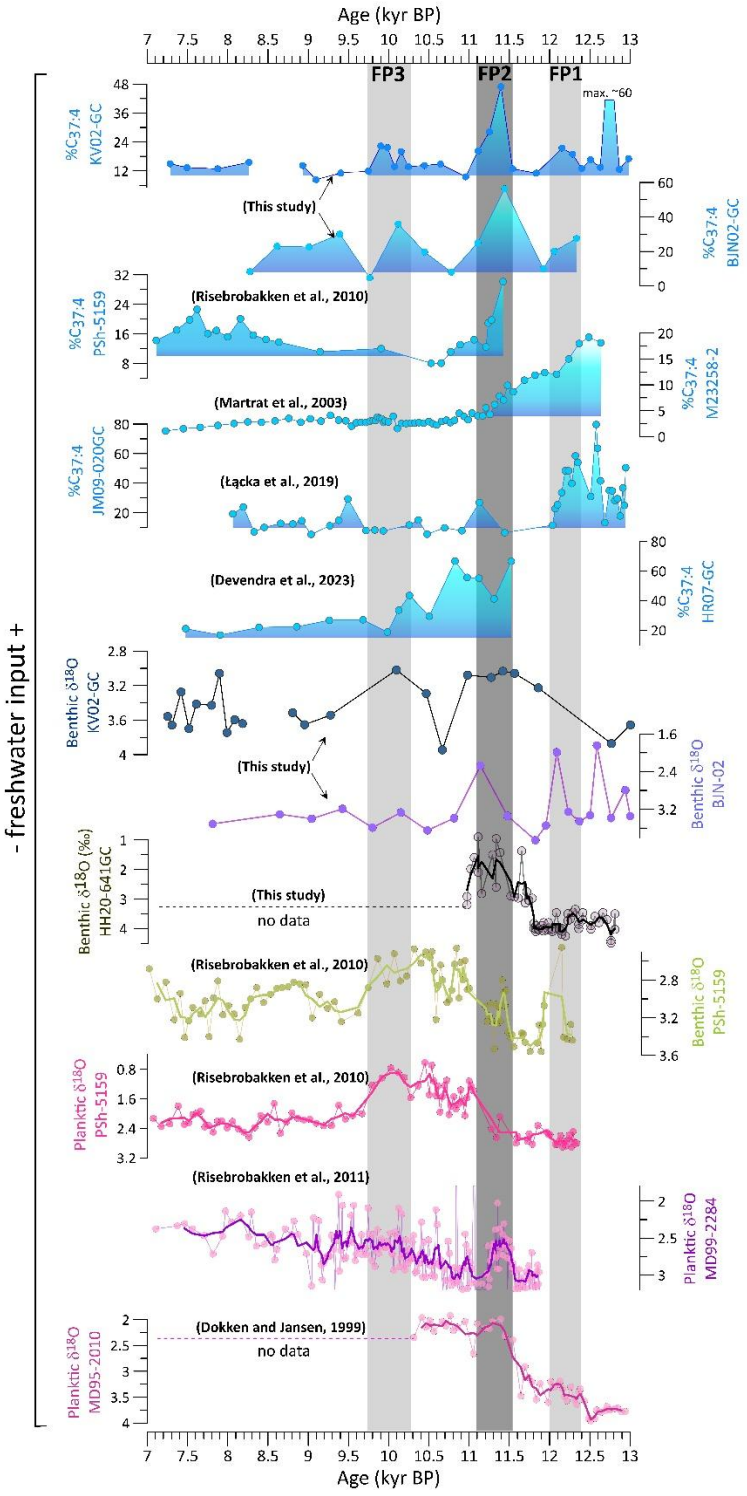



**Figure 4. Comparison of proxy records of the tetra-unsaturated alkenone fraction (%$C_{37:4}$), planktic and benthic $\delta^{18}O$ from gravity cores KV02-GC, BJN02-GC, and HH20-641GC (this study) with reference cores:** PSh-5159 [22], M23258-2 [18, 19], JM09-020GC [21], HR07-GC [13], MD99-2284 [25], and MD95-2010 [23]. Blue vertical bars indicate freshwater events FP1–FP3 identified in this study, with the darker bar marking the Preboreal Oscillation-related event. The data-free interval in KV02-GC corresponds to a reworked sediment layer identified by Devendra,

Łącka [32].

Freshwater input may have disrupted the northward advection of Atlantic Water, shifting the Arctic Front westward from the Norwegian Sea and western Barents Sea continental margin, as recorded by Risebrobakken and Berben [44]. This shift, along with the increased planktic–benthic $\delta^{13}C$ regional offset that reflects weak ventilation (Fig. S1), highlights a broader regional reorganization of hydrography and ocean circulation during this time.

**Potential freshwater triggers for the Preboreal cooling**

The PBO has long been linked to an influx of freshwater into the North Atlantic, which weakened thermohaline circulation and led to cooling [14, 15, 17, 45]. However, the exact source of this freshwater remains debatable. Hald and Hagen [15] proposed that meltwater from retreating glacial margins around the Nordic Seas during the post-YD warming triggered the PBO. However, we consider this hypothesis alone unlikely, as it fails to explain the brevity of the event and the absence of similar events despite the continued presence of ice sheets in the region.

As a potential contributor, Fisher, Smith [17] proposed an outburst from Lake Agassiz via the Mackenzie River into the Arctic Ocean. They argued that this large freshwater discharge could have enhanced winter ice production, promoted thicker pack-ice growth across the Arctic, and facilitated the southward export of sea-ice (and its associated freshwater), thereby triggering the PBO. However, these interpretations were made without the support of robust sea-ice proxy data. Recent studies from the Fram Strait indicate that, since the YD, the region experienced a significant retreat of the sea-ice cover, as evidenced by high brassicasterol concentrations and minimum $IP_{25}$ concentrations in the Fram Strait [46, 47]. Thus, while the Agassiz outburst may have contributed to the PBO, an additional freshwater source is required to explain the timing and magnitude of the PBO.

We argue that the distinct FP2 event documented in this study represents a major freshwater forcing episode associated with an outburst of the Baltic Ice Lake (BIL; Fig. 1) that likely contributed to the PBO. The final drainage of the BIL across the Mount Billingen threshold after the YD (10 $^{14}C$ kyr; 11.5 kyr BP; Fig. 1) has delivered freshwater towards the North Sea and the North Atlantic [1, 45, 48, 49, 50]. With a computed area of ~ 0.35 million $km^2$ and a volume of ~ 30,000 $km^3$ [49], the BIL ranks among the largest known ice-dammed lakes of the period, comparable in size to Lake Agassiz at its Upper Campbell level (~9,400 $^{14}C$ yr BP), which Leverington, Mann [51]

243 estimated to have an area of ~ 0.26 million km$^2$ and a volume of ~ 23,000 km$^3$. Catastrophic BIL
244 drainage, estimated at ~ 7,800 km$^3$ over 1 - 2 years [14, 49], delivered a significant volume of fresh
245 water directly into the Nordic Seas. This event lowered the BIL level by 25 meters and reduced its
246 area by at least 18%, which is equivalent to ~ 0.062 million km$^2$ [49].

247 Coupled with marine evidence from a south-to-north transect (60°–75°N: Fig. 1) in the
248 Norwegian Sea and western Barents Sea, which shows distinct signals of surface freshening and
249 concomitant cooling (Figs. 4 and 5), our findings suggest that the BIL outburst likely contributed
250 directly to surface freshening in the North Atlantic. This freshwater input may have played a critical
251 role in amplifying, or even initiating, the PBO cooling. While some earlier studies have suggested
252 this possibility [12, 14, 15], they lacked the support of robust regional proxies. Based on the freshwater
253 proxies and regional correlations presented here, we propose that the FP2 event, linked to the BIL
254 outburst, represents a previously underappreciated yet crucial driver of early Holocene ocean
255 freshening and the onset of Preboreal cooling.
256

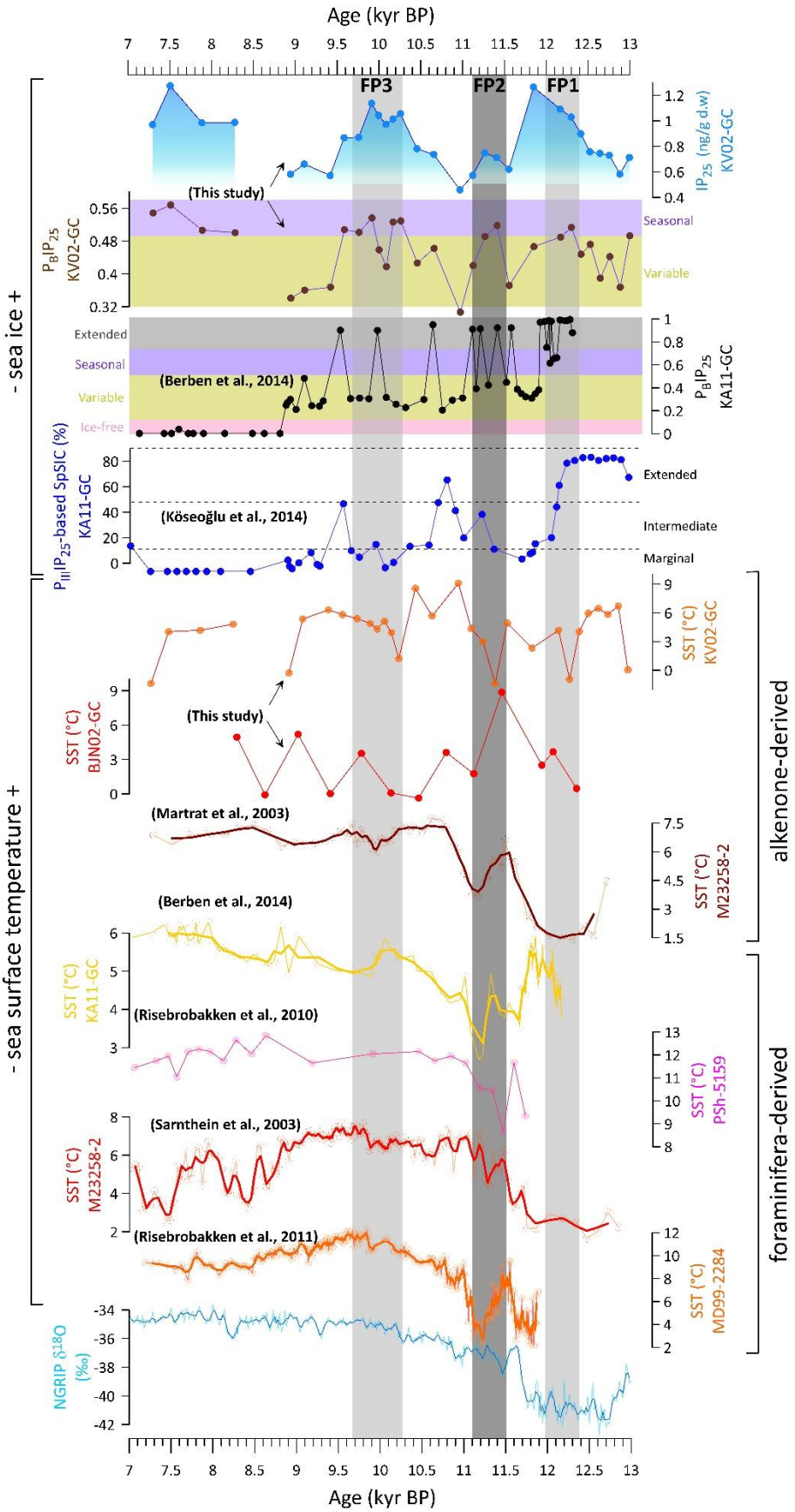

Age (kyr BP)
7
7.5
8
8.5
9
9.5
10
10.5
11
11.5
12
12.5
13
FP3
FP2
FP1
- sea ice +
- sea surface temperature +
IP25 (ng/g d.w) KV02-GC
(This study)
PBIP25 KV02-GC
Seasonal
Variable
Extended
Seasonal
Variable
Ice-free
(Berben et al., 2014)
PBIP25 KA11-GC
PIIIIP25-based SpSIC (%) KA11-GC
(Köseoğlu et al., 2014)
Extended
Intermediate
Marginal
SST (°C) KV02-GC
SST (°C) BJN02-GC
(This study)
(Martrat et al., 2003)
SST (°C) M23258-2
(Berben et al., 2014)
SST (°C) KA11-GC
(Risebrobakken et al., 2010)
SST (°C) PSh-5159
(Sarnthein et al., 2003)
SST (°C) M23258-2
(Risebrobakken et al., 2011)
SST (°C) MD99-2284
NGRIP δ18O (‰)
alkenone-derived
foraminifera-derived
Age (kyr BP)

**Figure 5. Comparison of proxy records of the $IP_{25}$ and $PBIP_{25}$ (sea-ice indicators), and reconstructed sea-surface temperature (SST) from cores KV02-GC and BJN02-GC (this study) with reference cores:** KA11-GC [20, 52], M23258-2 [18, 19], PSh-5159 [22], and MD99-2284 [25]. Blue vertical bars indicate freshwater events FP1–FP3 identified in this study, with the darker bar marking the Preboreal Oscillation-related event. The data-free interval in KV02-GC corresponds to a reworked sediment layer identified by Devendra, Łącka [32].

**Table 1**. AMS $^{14}C$ measurements and calibrated ages of core **OCE23-BJN02-GC, OCE22-KV02-GC,** and **HH20-641GC** applying the Marine20 calibration curve. Median ages (in bold) were used for the age-depth model. Calibrated ages are reported in thousands of years before AD 1950 (years BP). The red italicized dates indicate the Storegga tsunami-reworked sediment layer identified in core **OCE22-KV02-GC** [32].

| Lab ID | Depth (cm) | Dated material | $^{14}C$ age | Calibrated age (year BP, 2σ) | | |
|---|---|---|---|---|---|---|
| | | | | Min age | Max age | Median age |
| ***OCE23-BJN02-GC*** | | | | | | |
| 13971.1.1 | 9 | *Cibicidoides lobatulus* | 3941 ± 71 | 3621 | 4136 | **3875** |
| 14449.1.1 | 22 | Mixed benthic foraminifera | 7181 ± 92 | 7338 | 7787 | **7560** |
| 14153.1.1 | 35 | Mixed benthic foraminifera | 10567 ± 101 | 11399 | 12233 | **11815** |
| 14154.1.1 | 44 | Mixed benthic foraminifera | 11630 ± 104 | 12776 | 13290 | **13040** |
| 13972.1.1 | 57 | Mixed benthic foraminifera | 11744 ± 115 | 12876 | 13442 | **13160** |
| 13973.1.1 | 85 | Mixed benthic foraminifera | 12850 ± 116 | 14144 | 15043 | **14615** |
| 13974.1.1 | 128 | Mixed benthic foraminifera | 16690 ± 177 | 18876 | 19839 | **19345** |
| ***OCE22-KV02-GC*** | | | | | | |
| 11617.1.1 | 3 | Mixed benthic foraminifera | 2830 ± 80 | 2282 | 2751 | **2520** |
| 11348.1.1 | 21 | Mixed benthic foraminifera | 6910 ± 80 | 7099 | 7518 | **7315** |
| 11619.1.1 | 39 | Mixed benthic foraminifera | 7700 ± 125 | 7788 | 8363 | **8075** |
| 14834.1.1 | 41 | Mixed benthic foraminifera | *10650 ± 120* | *11521* | *12421* | *11955* |
| 14609.1.1 | 48 | Mixed benthic foraminifera | *12400 ± 130* | *13503* | *14331* | *13905* |
| 11349.1.1 | 53 | Mixed benthic foraminifera | *23720 ± 280* | *26560* | *27707* | *27190* |
| 14610.1.1 | 55 | Mixed benthic foraminifera | *13395 ± 140* | *14996* | *15843* | *15415* |
| 14836.1.1 | 59 | Mixed benthic foraminifera | *10870 ± 125* | *11863* | *12617* | *12265* |
| 11620.1.1 | 61 | Mixed benthic foraminifera | 8200 ± 140 | 8280 | 9033 | **8645** |
| 11350.1.1 | 81 | Mixed benthic foraminifera | 9575 ± 105 | 10104 | 10754 | **10405** |
| 14611.1.1 | 94 | Mixed benthic foraminifera | 10905 ± 125 | 11920 | 12650 | **12310** |
| 11350.1.2 | 130 | Mixed benthic foraminifera | 12625 ± 145 | 13790 | 14812 | **14265** |
| 11622.1.1 | 137 | *Elphidium clavatum* | 12810 ± 195 | 13915 | 15171 | **14550** |
| ***HH20-641GC*** | | | | | | |
| HH20-641_108.5 | 108.5 | *Arctica islandica* | 8103 ± 32 | 8162 | 8529 | **8400** |
| HH20-641_349 | 348-350 | *Arctica islandica* | 9779 ± 31 | 10280 | 10662 | **10452** |
| HH20-641_511 | 511 | *Nucula sp* | 10703 ± 34 | 11710 | 12210 | **11875** |

## Methods

### Coring

Gravity sediment cores OCE2022-KV02-GC (KV02-GC) and OCE2023-BJN02-GC (BJN02-GC) were retrieved from the western Barents Sea during the AREX expedition aboard R/V *Oceania* in August 2022 and 2023, respectively. The core sites were located at 74°50.296N, 16°1.3403E (374 m water depth) and 72°22.496N, 16°54.856E (375 m water depth), respectively (Fig. 1). Additionally, gravity sediment core HH20-641GC was collected from Kvalsund near Kvaløya, northern Norway, aboard R/V Helmer Hanssen in October 2020. The core site was located at 69°56.043N, 18°35.311E at a water depth of 272 m (Fig. 1).

### AMS-$^{14}$C dating and age-depth model

The age–depth models for cores KV02-GC and BJN02-GC are based on eight and seven radiocarbon dates, respectively, measured at the MICADAS facility at the Alfred Wegener Institute, Bremerhaven, Germany (Fig. S2; Table 1). The resulting raw radiocarbon dates were calibrated to calendar ages in the CALIB $^{14}$C software ((8.2.0; Stuiver, Reimer [53]) using the Marine20 dataset [54] and applying a regional radiocarbon reservoir offset (ΔR) of -92 ± 34 years. This ΔR value corresponds to 67 ± 34 years relative to the Marine04 calibration curve based on data from the vicinity of Bear Island [55]. The ΔR value relative to the Marine20 calibration curve was calculated using the Marine Reservoir Correction database [56].

For core HH20-641GC, collected from Kvalsund near Kvaløya, northern Norway, the radiocarbon dates were calibrated using the same Marine20 dataset, but applying a regional reservoir correction (ΔR) of −100 ± 37 years [55] relative to the Marine20 calibration curve.

The Bayesian age-depth modeling program Bacon 4.4.3 [57] in R statistical software was used to develop a suitable age model for sediment cores KV02-GC, BJN02-GC, and HH20-641GC (Fig. S2).

### Stable isotopes

For cores KV02-GC and BJN02-GC, stable isotope analyses were performed on the benthic species E. clavatum, picked from the 100–500 µm size fraction. The measurements were performed

using a Thermo Finnigan MAT 252 mass spectrometer with a Kiel III automatic carbonate preparation device at the Light Stable Isotope Mass Spec Laboratory, Department of Geological Sciences, University of Florida, USA. Measurement precision was better than ±0.04‰ and ±0.02‰ for oxygen and carbon isotopes, respectively.

For core HH20-641GC, a continuous isotope record was generated using three benthic foraminiferal species (*Nonionellina labradorica, Cassidulina reniforme*, and *Cibicidoides lobatulus*). Isotopic measurements were performed using a Thermo Scientific MAT253 isotope ratio mass spectrometer (IRMS) coupled to a GasBench II preparation system at the Department of Geosciences, UiT The Arctic University of Norway, Tromsø. The analytical precision of the instrument is ±0.1‰ for both oxygen and carbon isotopes, and results are reported relative to an in-house Vienna Pee Dee Belemnite (VPDB) standard.

**Biomarker analysis**

Lipid biomarkers were analyzed using the procedures described in detail by Krajewska, Lubecki [58] and Szymczak-Żyła and Lubecki [59], with some modifications. Freeze-dried samples (~ 4 g) spiked with surrogate standards (9-octylheptadecene, 7-hexylnonadecane, 2-nonadecanone, and androstanol) were sonication-extracted with a dichloromethane : methanol (2:1 v/v) mixture (3 x 15 ml). After extraction, the raw extracts were concentrated using rotary evaporation and divided into two subsamples (A and B).

Subsample A was fractionated by solid-phase extraction (SPE) using 1% deactivated silica gel. The fraction containing highly branched isoprenoid ($IP_{25}$) was eluted with a hexane and dichloromethane (1:1 v/v) mixture, whereas the fraction containing alkenones was eluted with dichloromethane. $IP_{25}$ was analyzed using a gas chromatograph coupled to a quadrupole mass spectrometer detector (GC-MS-QP2010 Ultra; Shimadzu) according to the procedure described in Krajewska, Lubecki [58]. The concentrations of $IP_{25}$ were calculated based on response factors for $IP_{25}$ and the standards, following the procedure described by Belt, Brown [60]. Alkenones were analyzed using a gas chromatograph with a flame ionization detector (GC/FID; Nexis GC-2030, Shimadzu) [58].

To determine the total (free + esterified) sterols, subsample B was saponified with 5% KOH in methanol, and then liquid-liquid extraction was performed using the KOH–methanol

extract/chloroform/water system (1/3/2 v/v/v) three times. The combined chloroform fractions were concentrated by rotary evaporation, derivatized to produce the trimethylsilyl derivatives, and analyzed using a gas chromatograph coupled to a mass spectrometer detector (GC-MS-QP2010 Ultra; Shimadzu) according to the procedure described by Szymczak-Żyła and Lubecki [59]. The analytes were identified based on their retention times and mass spectra and quantified based on response factors derived from daily injections of standard mixtures. The following sterols were studied: 24-methylenecholosterol, brassicasterol, and dinosterol.

The $P_BIP_{25}$ index was calculated by combining $IP_{25}$ with another phytoplankton marker – brassicasterol – to reconstruct sea ice conditions using the following equation [61]:

$$P_BIP_{25} = IP_{25}/ (IP_{25} + (p \times c))$$

where $p$ is the phytoplankton marker concentration (brassicasterol), and c is a balance factor (mean $IP_{25}$ concentration/mean $p$ concentration).

The $U^K_{37}$ index was used to estimate the sea surface temperature (SST). To prevent negative SST values resulting from the high abundance of tetra-unsaturated alkenone ($C_{37:4}$) in our samples, we applied the following equation to calculate the $U^K_{37}$ index introduced by Bendle and Rosell-Melé [62]:

$$U^{K*}_{37} = [C_{37:2}]/([C_{37:2}] + [C_{37:3}] + [C_{37:4}])$$

$U^{K*}_{37}$ values were converted to SSTs using global core-top calibration, as indicated by the following equation [63]:

$$SST= (U^{K*}_{37} - 0.243)/0.021$$

**Author contributions.** DD, MŁ, NS, and MZ conceptualized the study. MZ and MŁ supervised the research. DD performed data curation, formal analysis, age-model development, visualization, and wrote the original draft. NS, MŁ, MMT, PDS, MS-Ż, and MK contributed to formal analysis. TLR provided radiocarbon dating data for core HH20-641GC. TLR and KM conducted stable

isotope analyses of core HH20-641GC. All authors contributed to data interpretation, manuscript review, and editing.

**Competing interest.** The authors declare no conflicts of interest.

**Acknowledgments.** We want to thank Agnieszka Kujawa for helping with the foraminiferal identifications. Special thanks to Prof. Simon T. Belt and Dr. Lukas Smik (University of Plymouth, UK) for providing reference sediment and standards for $IP_{25}$ analyses. We also extend our gratitude to the R/V *Oceania* crew, who helped during sediment core retrieval.

**Financial support.** The research was financially supported by the National Science Centre, Poland, project no. 2025/57/B/ST10/02651. MZ and NS were supported by the National Science Centre, Poland, project no. 2023/51/B/ST10/01579. ML and DD were supported by the National Science Centre, Poland, project no. 2022/45/B/ST10/02033. Support for this work also came from the Johanna M. Resig Fellowship granted to DD by the Cushman Foundation.

## References

1. Nesje, A., Dahl, S. O. & Bakke, J. Were abrupt Lateglacial and early-Holocene climatic changes in northwest Europe linked to freshwater outbursts to the North Atlantic and Arctic Oceans? *The Holocene* **14**, 299–310 https://doi.org/10.1191/0959683604hl708fa (2004).

2. Harrison, S., Smith, D. E. & Glasser, N. F. Late Quaternary meltwater pulses and sea level change. *Journal of Quaternary Science* **34**, 1–15 https://doi.org/10.1002/jqs.3070 (2018).

3. You, D.*, et al.* Last deglacial abrupt climate changes caused by meltwater pulses in the Labrador Sea. *Communications Earth & Environment* **4**, https://doi.org/10.1038/s43247-023-00743-3 (2023).

4. Lehman, S. J. & Keigwin, L. D. Sudden Changes in North-Atlantic Circulation during the Last Deglaciation. *Nature* **356**, 757–762 https://doi.org/DOI 10.1038/356757a0 (1992).

5. Koc, N., Jansen, E. & Haflidason, H. Paleoceanographic Reconstructions of Surface Ocean Conditions in the Greenland, Iceland and Norwegian Seas through the Last 14-Ka Based on Diatoms. *Quaternary Science Reviews* **12**, 115–140 https://doi.org/Doi 10.1016/0277-3791(93)90012-B (1993).

6. Tuckett, P. A.*, et al.* Automated mapping of the seasonal evolution of surface meltwater and its links to climate on the Amery Ice Shelf, Antarctica. *The Cryosphere Discussions* **2021**, 1–35 (2021).

7. Ackermann, L., Danek, C., Gierz, P. & Lohmann, G. AMOC Recovery in a multicentennial scenario using a coupled atmosphere-ocean-ice sheet model. *Geophysical Research Letters* **47**, e2019GL086810 (2020).

8. Alsos, I. G.*, et al.* Postglacial species arrival and diversity buildup of northern ecosystems took millennia. *Sci Adv* **8**, eabo7434 https://doi.org/10.1126/sciadv.abo7434 (2022).

9. Nobre, P.*, et al.* AMOC decline and recovery in a warmer climate. *Scientific Reports* **13**, 15928 (2023).

10. Li, Q.*, et al.* Global climate impacts of Greenland and Antarctic meltwater: A comparative study. *Journal of Climate* **36**, 3571–3590 (2023).

11. Lohmann, J. & Ditlevsen, P. D. Risk of tipping the overturning circulation due to increasing rates of ice melt. *Proceedings of the National Academy of Sciences* **118**, e2017989118 (2021).

12. Björck, S., Rundgren, M., Ingólfsson, Ó. & Funder, S. The Preboreal oscillation around the Nordic Seas: terrestrial and lacustrine responses. *Journal of Quaternary Science* **12**, 455–465 https://doi.org/10.1002/(sici)1099-1417(199711/12)12:6<455::Aid-jqs316>3.0.Co;2-s (1997).

13. Devendra, D.*, et al.* The development of ocean currents and the response of the cryosphere on the Southwest Svalbard shelf over the Holocene. *Global and Planetary Change* **228**, https://doi.org/10.1016/j.gloplacha.2023.104213 (2023).

14. Björck, S.*, et al.* Synchronized Terrestrial-Atmospheric Deglacial Records Around the North Atlantic. *Science* **274**, 1155–1160 https://doi.org/10.1126/science.274.5290.1155 (1996).

15. Hald, M. & Hagen, S. Early preboreal cooling in the Nordic seas region triggered by meltwater. *Geology* **26**, 615–618 https://doi.org/Doi 10.1130/0091-7613(1998)026<0615:Epcitn>2.3.Co;2 (1998).

16. Bos, J. A. A., van Geel, B., van der Plicht, J. & Bohncke, S. J. P. Preboreal climate oscillations in Europe: Wiggle-match dating and synthesis of Dutch high-resolution multi-proxy records. *Quaternary Science Reviews* **26**, 1927–1950 https://doi.org/10.1016/j.quascirev.2006.09.012 (2007).

17. Fisher, T. G., Smith, D. G. & Andrews, J. T. Preboreal oscillation caused by a glacial Lake Agassiz flood. *Quaternary Science Reviews* **21**, 873–878 https://doi.org/Pii S0277-3791(01)00148-2

Doi 10.1016/S0277-3791(01)00148-2 (2002).

18. Martrat, B., Grimalt, J. O., Villanueva, J., van Kreveld, S. & Sarnthein, M. Climatic dependence of the organic matter contributions in the north eastern Norwegian Sea over the last 15,000 years. *Organic Geochemistry* **34**, 1057–1070 https://doi.org/10.1016/s0146-6380(03)00084-6 (2003).

19. Sarnthein, M., *et al.* Centennial-to-millennial-scale periodicities of Holocene climate and sediment injections off the western Barents shelf, 75°N. *Boreas* **32**, 447–461 https://doi.org/10.1080/03009480310003351 (2003).

20. Berben, S. M. P., Husum, K., Cabedo-Sanz, P. & Belt, S. T. Holocene sub-centennial evolution of Atlantic water inflow and sea ice distribution in the western Barents Sea. *Climate of the Past* **10**, 181–198 https://doi.org/10.5194/cp-10-181-2014 (2014).

21. Łącka, M., *et al.* Postglacial paleoceanography of the western Barents Sea: Implications for alkenone-based sea surface temperatures and primary productivity. *Quaternary Science Reviews* **224**, https://doi.org/10.1016/j.quascirev.2019.105973 (2019).

22. Risebrobakken, B., Moros, M., Ivanova, E. V., Chistyakova, N. & Rosenberg, R. Climate and oceanographic variability in the SW Barents Sea during the Holocene. *The Holocene* **20**, 609–621 https://doi.org/10.1177/0959683609356586 (2010).

23. Dokken, T. M. & Jansen, E. Rapid changes in the mechanism of ocean convection during the last glacial period. *Nature* **401**, 458–461 https://doi.org/Doi 10.1038/46753 (1999).

24. Risebrobakken, B., Jansen, E., Andersson, C., Mjelde, E. & Hevrøy, K. A high-resolution study of Holocene paleoclimatic and paleoceanographic changes in the Nordic Seas. *Paleoceanography* **18**, https://doi.org/10.1029/2002pa000764 (2003).

25. Risebrobakken, B., *et al.* Early Holocene temperature variability in the Nordic Seas: The role of oceanic heat advection versus changes in orbital forcing. *Paleoceanography* **26**, https://doi.org/10.1029/2011pa002117 (2011).

26. Ryan, W. B., *et al.* Global multi-resolution topography synthesis. *Geochemistry, Geophysics, Geosystems* **10**, (2009).

27. Bard, E., Rostek, F., Turon, J. L. & Gendreau, S. Hydrological impact of heinrich events in the subtropical northeast atlantic. *Science* **289**, 1321–1324 https://doi.org/10.1126/science.289.5483.1321 (2000).

28. Prahl, F. G. & Wakeham, S. G. Calibration of unsaturation patterns in long-chain ketone compositions for palaeotemperature assessment. *Nature* **330**, 367–369 https://doi.org/10.1038/330367a0 (1987).

29. Bendle, J., Rosell-Melé, A. & Ziveri, P. Variability of unusual distributions of alkenones in the surface waters of the Nordic seas. *Paleoceanography* **20**, https://doi.org/10.1029/2004pa001025 (2005).

30. Wang, K. J., *et al.* Group 2i Isochrysidales produce characteristic alkenones reflecting sea ice distribution. *Nat Commun* **12**, 15 https://doi.org/10.1038/s41467-020-20187-z (2021).

31. Rosell-Melé, A., Jansen, E. & Weinelt, M. Appraisal of a molecular approach to infer variations in surface ocean freshwater inputs into the North Atlantic during the last glacial. *Global and Planetary Change* **34**, 143–152 https://doi.org/Pii S0921-8181(02)00111-X

Doi 10.1016/S0921-8181(02)00111-X (2002).

32. Devendra, D., *et al.* Expanding the footprint of the Storegga tsunami through new evidence from Arctic marine sediments. *Scientific Reports* **15**, https://doi.org/10.1038/s41598-025-10811-7 (2025).

33. Łącka, M., Zajączkowski, M., Forwick, M. & Szczuciński, W. Late Weichselian and Holocene palaeoceanography of Storfjordrenna, southern Svalbard. *Climate of the Past* **11**, 587–603 https://doi.org/10.5194/cp-11-587-2015 (2015).

34. Rasmussen, T. L. & Thomsen, E. The role of the North Atlantic Drift in the millennial timescale glacial climate fluctuations. *Palaeogeogr Palaeocl* **210**, 101–116 https://doi.org/10.1016/j.palaeo.2004.04.005 (2004).

35. Hald, M., *et al.* Recent and Late Quaternary distribution of Elphidium excavatum f. clavatum in Arctic seas. (1994).

36. Detlef, H., *et al.* Late quaternary sea-ice and sedimentary redox conditions in the eastern Bering Sea – Implications for ventilation of the mid-depth North Pacific and an Atlantic-Pacific seesaw mechanism. *Quaternary Science Reviews* **248**, https://doi.org/10.1016/j.quascirev.2020.106549 (2020).

37. Volkman, J. K. A review of sterol markers for marine and terrigenous organic matter. *Organic geochemistry* **9**, 83–99 (1986).

38. Boon, J. J., *et al.* Black Sea sterol—a molecular fossil for dinoflagellate blooms. *Nature* **277**, 125–127 (1979).

39. Belt, S. T., Brown, T. A., Smik, L., Assmy, P. & Mundy, C. Sterol identification in floating Arctic sea ice algal aggregates and the Antarctic sea ice diatom Berkeleya adeliensis. *Organic Geochemistry* **118**, 1–3 (2018).

40. Smith Jr, W. O. & Sakshaug, E. Polar phytoplankton. In: *Polar oceanography*). Elsevier (1990).

41. Hald, M., *et al.* Variations in temperature and extent of Atlantic Water in the northern North Atlantic during the Holocene. *Quaternary Science Reviews* **26**, 3423–3440 https://doi.org/10.1016/j.quascirev.2007.10.005 (2007).

42. Rasmussen, T. L., *et al.* Spatial and temporal distribution of Holocene temperature maxima in the northern Nordic seas: interplay of Atlantic-, Arctic- and polar water masses. *Quaternary Science Reviews* **92**, 280–291 https://doi.org/10.1016/j.quascirev.2013.10.034 (2014).

43. El bani Altuna, N., *et al.* Deglacial bottom water warming intensified Arctic methane seepage in the NW Barents Sea. *Communications Earth & Environment* **2**, https://doi.org/10.1038/s43247-021-00264-x (2021).

44. Risebrobakken, B. & Berben, S. M. P. Early Holocene Establishment of the Barents Sea Arctic Front. *Frontiers in Earth Science* **6**, https://doi.org/10.3389/feart.2018.00166 (2018).

45. Bodén, P., Fairbanks, R. G., Wright, J. D. & Burckle, L. H. High-resolution stable isotope records from southwest Sweden: the drainage of the Baltic Ice Lake and Younger Dryas Ice Margin Oscillations. *Paleoceanography* **12**, 39–49 (1997).

46. Müller, J. & Stein, R. High-resolution record of late glacial and deglacial sea ice changes in Fram Strait corroborates ice–ocean interactions during abrupt climate shifts. *Earth and Planetary Science Letters* **403**, 446–455 https://doi.org/10.1016/j.epsl.2014.07.016 (2014).

47. Müller, J., Massé, G., Stein, R. & Belt, S. T. Variability of sea-ice conditions in the Fram Strait over the past 30,000 years. *Nature Geoscience* **2**, 772–776 https://doi.org/10.1038/ngeo665 (2009).

48. Bjorck, S. A Review of the History of the Baltic Sea, 13.0-8.0 Ka Bp. *Quaternary International* **27**, 19–40 https://doi.org/Doi 10.1016/1040-6182(94)00057-C (1995).

49. Jakobsson, M., *et al.* Reconstructing the Younger Dryas ice dammed lake in the Baltic Basin: Bathymetry, area and volume. *Global and Planetary Change* **57**, 355–370 https://doi.org/10.1016/j.gloplacha.2007.01.006 (2007).

50. Stroeven, A. P., *et al.* A new Scandinavian reference 10Be production rate. *Quaternary Geochronology* **29**, 104–115 https://doi.org/10.1016/j.quageo.2015.06.011 (2015).

51. Leverington, D. W., Mann, J. D. & Teller, J. T. Changes in the bathymetry and volume of glacial Lake Agassiz between 11,000 and 9300 14C yr BP. *Quaternary Research* **54**, 174–181 (2000).

52. Köseoğlu, D., Belt, S. T., Husum, K. & Knies, J. An assessment of biomarker-based multivariate classification methods versus the PIP25 index for paleo Arctic sea ice reconstruction. *Organic Geochemistry* **125**, 82–94 https://doi.org/10.1016/j.orggeochem.2018.08.014 (2018).

53. Stuiver, M., Reimer, P. J. & Reimer, R. W. CALIB 8.2 [WWW program] at http://calib.org, accessed 2022-2-25. (2022).

54. Heaton, T. J., *et al.* Marine20—The Marine Radiocarbon Age Calibration Curve (0–55,000 cal BP). *Radiocarbon* **62**, 779–820 https://doi.org/10.1017/rdc.2020.68 (2020).

55. Mangerud, J. & Gulliksen, S. Apparent radiocarbon ages of recent marine shells from Norway, Spitsbergen, and Arctic Canada. *Quaternary Research* **5**, 263–273 (1975).

56. Reimer, P. J. & Reimer, R. W. A marine reservoir correction database and on-line interface. *Radiocarbon* **43**, 461–463 (2001).

57. Blaauw, M. & Christen, J. A. Flexible paleoclimate age-depth models using an autoregressive gamma process. *Bayesian Analysis* **6**, https://doi.org/10.1214/11-ba618 (2011).

58. Krajewska, M., Lubecki, L. & Szymczak-Żyła, M. Sources of sedimentary organic matter in Arctic fjords: Evidence from lipid molecular markers. *Continental Shelf Research* **264**, https://doi.org/10.1016/j.csr.2023.105053 (2023).

59. Szymczak-Żyła, M. & Lubecki, L. Biogenic and anthropogenic sources of sedimentary organic matter in marine coastal areas: A multi-proxy approach based on bulk and molecular markers. *Marine Chemistry* **239**, https://doi.org/10.1016/j.marchem.2021.104069 (2022).

60. Belt, S. T.*, et al.* A reproducible method for the extraction, identification and quantification of the Arctic sea ice proxy IP 25 from marine sediments. *Analytical methods* **4**, 705–713 (2012).

61. Müller, J.*, et al.* Towards quantitative sea ice reconstructions in the northern North Atlantic: A combined biomarker and numerical modelling approach. *Earth and Planetary Science Letters* **306**, 137–148 https://doi.org/10.1016/j.epsl.2011.04.011 (2011).

62. Bendle, J. & Rosell-Melé, A. Distributions of UK37 and UK37′ in the surface waters and sediments of the Nordic Seas: Implications for paleoceanography. *Geochemistry, Geophysics, Geosystems* **5**, https://doi.org/10.1029/2004gc000741 (2004).

63. Filippova, A., Kienast, M., Frank, M. & Schneider, R. R. Alkenone paleothermometry in the North Atlantic: A review and synthesis of surface sediment data and calibrations. *Geochemistry, Geophysics, Geosystems* **17**, 1370–1382 https://doi.org/10.1002/2015gc006106 (2016).

## Supplementary Files

This is a list of supplementary files associated with this preprint. Click to download.

- Supplementary.pdf
- DataKV02BJN02HH20PBO.xlsx